Received November 22, 2019, accepted December 14, 2019, date of publication January 3, 2020, date of current version January 24, 2020.

Digital Object Identifier 10.1109/ACCESS.2019.2963718

Analysis of Peak Electromagnetic Torque Characteristics for Superconducting DC Induction Heaters

PING YANG[1,3,4], SHAOTAO DAI[2], TAO MA[2], JIANMIN HUANG[3], GUOZHONG JIANG[3], YAWEI WANG[4], ZHIYONG HONG[4,5], AND ZHIJIAN JIN[4,5]

[1]Scientific Research Academy, Shanghai Maritime University, Shanghai 200135, China
[2]School of Electrical Engineering, Beijing Jiaotong University, Beijing 100044, China
[3]Jiangxi Lianchuang Opto-Electronic Science and Technology Company, Ltd., Nanchang 330096, China
[4]Department of Electrical Engineering, Shanghai Jiao Tong University, Shanghai 200240, China
[5]Shanghai Superconductor Technology Company, Ltd., Shanghai 201210, China

Corresponding author: Zhiyong Hong (zhiyong.hong@sjtu.edu.cn)

ABSTRACT The efficiency of novel superconducting direct current (DC) induction heaters can be up to 80-90%. This is much higher than the 40-50% of conventional alternating current induction heaters. Induction heaters are used to preheat aluminum billets in extrusion pressing. Such devices use a driving motor to rotate the billet. A peak in the electromagnetic torque appears at low rotation speeds (of the motor). Therefore, this peak electromagnetic torque is of particular interest when designing the driving system, which is one of the main challenges for megawatt-class superconducting DC induction heaters. In this paper, the peak electromagnetic torque characteristics of different sized billets were analyzed. A numerical 3D finite element method model was built to analyze the peak electromagnetic torque and resistive heating power behavior of aluminum billets. The results obtained from simulations and experiments match well. The effect of the following five relative parameters, on electromagnetic torque and resistive heating power, were studied: billet diameter, billet length, magnetic flux density, billet material, and electrical conductivity. The peak electromagnetic torque increases nonlinearly with increasing billet diameter, up to 640 mm. The time elapsed between the peak to stable torque decreases nonlinearly with increasing magnetic flux density. The effects of billet material (copper, titanium alloy and stainless steel) on torque were analyzed and compared. These results are likely to guide more cost-effective and practical designs for the billet driving system of superconducting DC induction heaters.

INDEX TERMS Superconducting DC induction heater, peak electromagnetic torque, aluminum billet, magnetic flux density.

I. INTRODUCTION

Induction heating has been widely used to preheat aluminum billets in extrusion pressing [1]–[3]. The superconducting direct current (DC) induction heating method can be much more efficient, in the metal preheating process, compared to traditional alternating current (AC) induction, when billets are made from low-resistivity and non-magnetic materials. Conventional AC induction heating devices generally have an efficiency of 40-45%, as a significant portion of energy is consumed to cool water for the copper coil [1]. High temperature superconductors (HTSs) show great advantages, in terms of energy conservation, because of their zero-resistance characteristics. They have been widely applied to improve energy efficiency in electrical devices, such as power cables, fault current limiters, and magnets [1], [4]–[19].

In commercial megawatt (MW) superconducting DC induction heaters, aluminum is rotated, by motors, in transverse magnetic fields. Peak electromagnetic torque occurs in the low-speed range, which tends to be 2.5 times that of the stable torque value. The peak electromagnetic torque in superconducting DC heaters has rarely been reported. It is now considered one of three main technical challenges for MW-class superconducting DC induction heaters [20], [21].

The associate editor coordinating the review of this manuscript and approving it for publication was Lei Chen.

This unique load characteristic makes selecting motors particularly difficult for this type of DC induction heater [22]–[24]. If the motor is selected according to its power and torque at its top-rated rotation speed (i.e. high speed), the billets will encounter a lack of torque during the start-up stage (i.e. low speed). If the motor was selected according to its peak torque at low speed, its high-power capability (about two thirds of the top-rated power) will be wasted at its high speed, which will considerably increase the cost of the heater. The first industry-scale HTS DC induction heater was developed in 2008, and was used to preheat Φ200 mm × 1000 mm aluminum billets [2]. In 2016, Choi et al. developed a 300 kW industry-scale superconducting DC induction heater for Φ236 mm × 1000 mm metal billets. In 2018, they also fabricated a commercial 300 kW superconducting induction heater [25]–[35]. The maximum billet size was Φ240 mm × 700 mm. Based on experimental and simulation results, the peak electromagnetic torque was not obvious for small diameter aluminum billets (<200 mm). The world's first commercial MW-class superconducting DC induction heater was proposed and developed by China in 2019 [4]–[7], [9], [13], [19]–[21], [24], [36]–[46]. It has been designed for aluminum billets with diameters of 200-446 mm and lengths of 80-1500 mm.

In this study, the peak electromagnetic torque characteristics of different billets, for superconducting DC induction heaters, were analyzed. A coupled 3D finite element method (FEM) model, using COMSOL Multiphysics software, was built to analyze the peak electromagnetic torque and the resistive heating power behavior of aluminum billets. Experimental measurements were carried out using an industrial MW-class superconducting DC induction heater. The experimental torque results confirmed the validity of our torque analysis method. The effect of five relative parameters, on electromagnetic torque and resistive heating power, were studied: billet diameter, billet length, magnetic flux density, billet material and electrical conductivity. Our peak electromagnetic torque characteristics results are useful for industrial applications of superconducting DC induction heaters. In particular, they may guide more cost-effective, practical and reliable driving system designs, to rotate aluminum billets heated by superconducting DC induction heaters.

II. ELECTROMAGNETIC TORQUE OF A SUPERCONDUCTING DC INDUCTION HEATER

A. PRINCIPLE OF A SUPERCONDUCTING DC INDUCTION HEATER

The superconducting DC induction heater was developed to avoid the AC losses of superconducting windings, as shown in Fig. 1. The aluminum billets are rotated by a driving motor, in a DC magnetic field generated by superconducting coils [47]–[49]. The superconducting magnet is used to generate an adjustable DC magnetic flux density of 0-1 T in the air gap of the iron core, where the aluminum billet is placed. The iron yoke is used to separate the HTS coils and heated billets, and to guide the magnetic flux to generate the desired field distribution [36]. DC current flows through the superconducting coils, thus, no AC loss is generated. The overall energy dissipations are losses in the motors and cooling system of the superconducting windings. Considering the high efficiency of motors (above 95%) and the low losses of superconducting DC coils, the overall energy efficiency can be up to 80-90% [50].

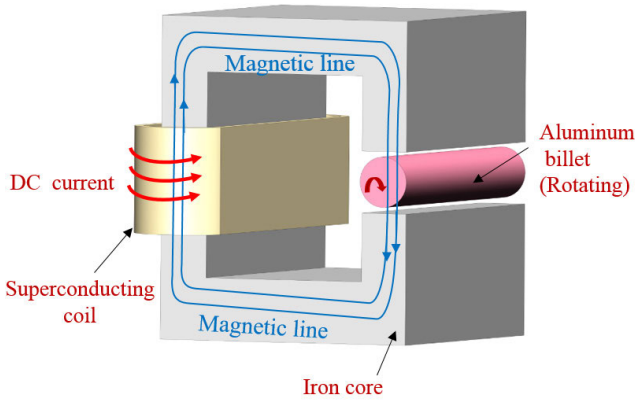

FIGURE 1. 3D schematic of the heating principle for superconducting DC induction heaters.

B. PEAK ELECTROMAGNETIC TORQUE

The electromagnetic torque of an aluminum billet is given by

$$\begin{cases} \tau = \int_{\partial\Omega} d(\mathrm{r} - \mathrm{r}_0) \times (nT)dS \\ \tau = \dfrac{\mathrm{r}_{ax}}{|\mathrm{r}_{ax}|} \cdot \tau \end{cases} \tag{1}$$

where τ is the electromagnetic torque, Ω is the computational domain, n is the normal vector, T is the surface stress tensor, r is the torque radius, r_0 is the torque rotation point, τ_{ax} is the torque axis, and r_{ax} is the torque around the x-axis [24].

The billet is rotated in transverse magnetic fields. Fig. 2 shows the electromagnetic torque dependency, and heating

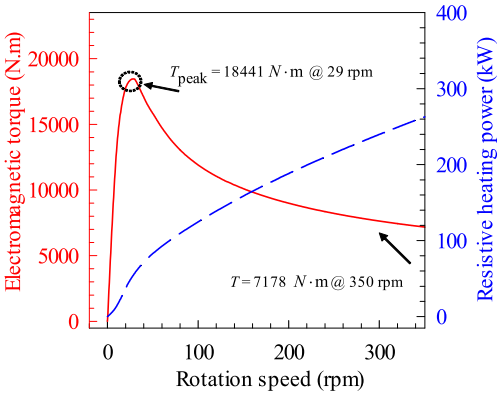

FIGURE 2. Simulation results of electromagnetic torque and resistive heating power versus rotational speed, for a Φ446 mm × 1335 mm aluminum billet in B = 0.3 T.

power on the billets, on the rotation speed. The data was acquired using Φ446 mm × 1335 mm aluminum billets in a magnetic field of 0.3 T. The results show that the induction heating power increases continually with rotation speed. The heating power of the top-rated speed (350 rpm) is 259 kW. However, the variation of electromagnetic torque shows a very different trend. It rapidly increases to its peak value at 29 rpm. It then drops quickly to a relatively small value, and subsequently decreases slowly as rotation speed increases. The peak electromagnetic torque is 18,441 N·m. Whereas the electromagnetic torque at 350 rpm is only 7,178 N·m, which is 39% of the peak value. However, for most motors, both the torque and power increases with rotation speed [24].

C. APPLICATIONS OF ALUMINUM BILLETS

The peak electromagnetic torque analysis of different aluminum billets is significant for various aluminum pressing applications, as shown in Fig. 3. Conventional AC inductance heaters can be divided into power frequency (50 or 60 Hz) and intermediate frequency (400-2,500 Hz) ranges, according to the power supply frequency. Aluminum billets with a diameter greater than 130 mm are heated by power frequency, while those with smaller diameters are heated by intermediate frequency. The rotational speed range of the superconducting DC induction heater is 240-480 rpm (corresponding frequency: 4-8 Hz). Therefore, the superconducting DC induction heater has a much greater range: 5-640 mm.

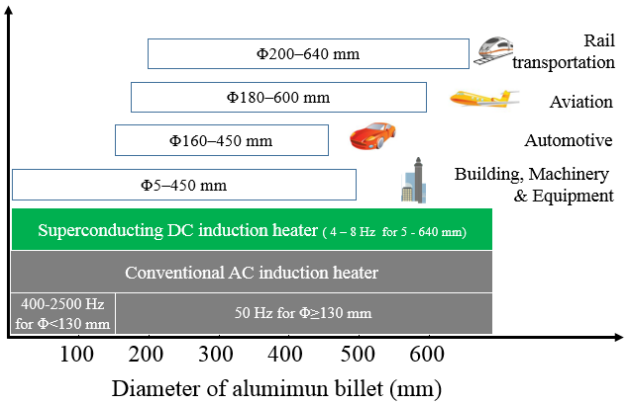

FIGURE 3. Applications of aluminum billets with different diameters of.

III. NUMERICAL MODEL AND VALIDATION

A. NUMERICAL MODEL

The coupled FEM numerical models include the meshed magnetic and electric fields model and heater transfer model, which are solved in COMSOL Multiphysics. When an aluminum billet is heated in the superconducting DC magnet, the billet is rotated in a static transverse magnetic field, to induce an eddy current, and is heated by Joule loss. In theory, this model is equivalent to a stationary billet placed in a rotating magnetic field with the same rotational frequency. The governing equations are

$$\begin{cases} B_x = B_0 \cos(\omega t) \\ B_y = B_0 \sin(\omega t) \end{cases} \tag{2}$$

where ω is the angular velocity of the rotating magnetic field, t is time and B_0 is the amplitude of the static magnetic field. According to Faraday's law of electromagnetic induction, the spatially changing magnetic field inside the aluminum billet will induce an electric field, such that

$$\nabla \times \mathrm{E}_i = -\frac{\partial B}{\delta t} \tag{3}$$

where E_i is the induced electric field and B is the magnetic field. When the rotational frequency of the magnetic field remains constant, or changes slowly, the change in the induced electric field over time will be negligible. Therefore, the spatial distribution of the electric field can be obtained according to Ampere's law:

$$\begin{cases} \nabla \times \mathrm{H} = J_i \\ J_i = \sigma \mathrm{E}_i \end{cases} \tag{4}$$

where σ is the conductivity and J_i is the induced eddy current. As the temperature changes, the electrical conductivity of the aluminum billet will change accordingly.

Fig. 4 shows the 3D geometry of the FEM model for a rotating aluminum billet in the magnetic flux field. Two subdomains are present in Fig. 4(a): the aluminum billet in the center and the air boundary. The majority of the eddy current and resistive heating power is distributed on the surface of the billet, due to the skin effect, so these areas are meshed more finely than others, as shown in Fig. 4(b). The aluminum billet has dimensions of Φ446 mm × 1500 mm and is meshed with 194,406 tetrahedral elements. The dimensions of the air boundary is Φ2000 mm × 6000 mm and is meshed with 805,382 tetrahedral elements.

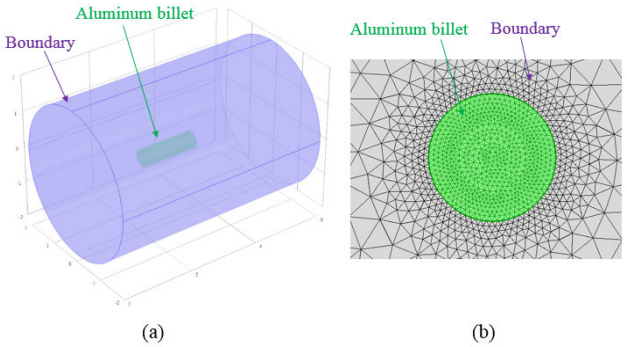

FIGURE 4. (a) 3D geometry of the FEM heating process model for a superconducting DC induction heater. (b) FEM model with mesh.

Fig. 5 presents the magnetic flux density and eddy current distribution for rotational speeds of 10 rpm and 500 rpm. Owing to the skin effect, the induced eddy current largely occurs on the surface of the aluminum billets. The radial eddy current density difference, of induction heating, depends on

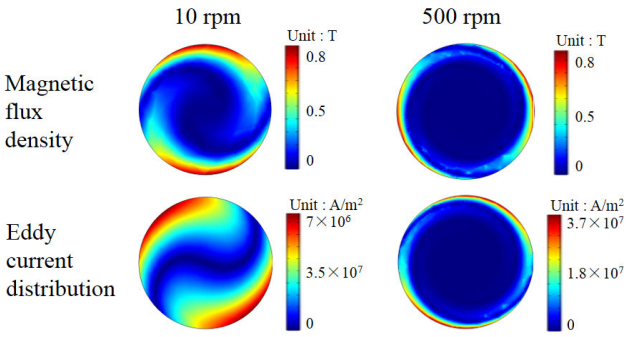

FIGURE 5. Comparison of magnetic flux density and eddy current distributions of the aluminum billet (Φ446 mm × 1500 mm), as a function of distance from the axis of symmetry, for 10 rpm and 500 rpm.

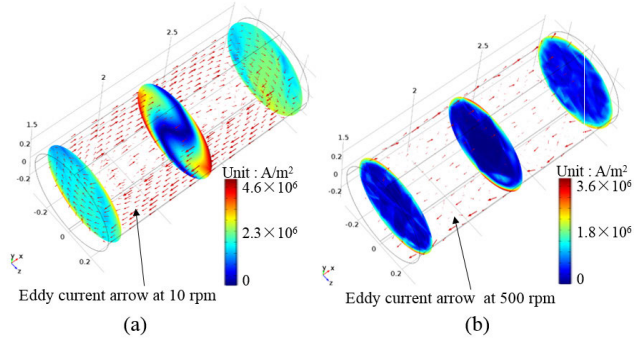

FIGURE 6. Induced eddy current density distribution (represented by arrows) of the aluminum billet (Φ446 mm × 1500 mm) at the rotational speed of (a) 10 rpm and (b) 500 rpm.

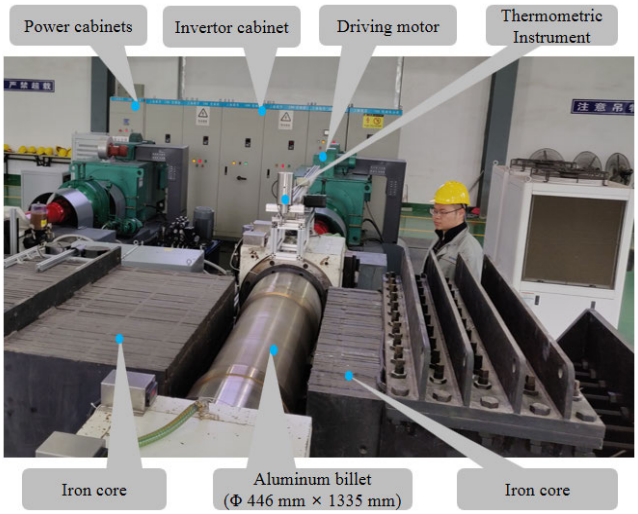

FIGURE 7. Image of aluminum billet (Φ446 mm × 1335 mm) during the heating process in the air gap of the iron core of the superconducting magnet.

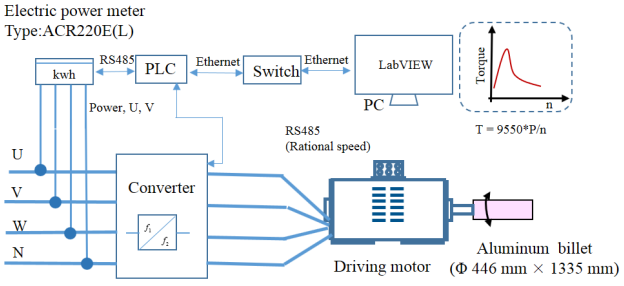

FIGURE 8. Schematic diagram of the real-time electromagnetic torque monitor system used to measure the real-time peak electromagnetic torque of aluminum billets during rotation.

the frequency: lower frequency results in deeper current penetration. Fig. 6 shows the induced eddy current density distributions, represented by arrows. The eddy current direction is axially oriented. This is different to that of the circumferential direction of the conventional AC induction heater. When the aluminum billet is rotated, the magnetic field in the air gap is formed by a superposition of the applied and the eddy current magnetic fields. The eddy current magnetic field is related to the rotational speed of the aluminum billet. The eddy current lines are concentrated nearer to the surface of the aluminum billet when the rotational speed is increased. Owing to the presence and demagnetization effect of the eddy current, the magnetic impedance of the magnetic circuit is increased, and the depth to which the magnetic flux penetrates into the aluminum is reduced.

B. TORQUE MEASUREMENT SYSTEM

To verify the peak electromagnetic torque, based on the 3D FEM model, experimental measurements were performed using the superconducting DC induction heater of a torque monitor system [21]. Fig. 7 shows an aluminum billet (446 mm × 1335 mm) in the air gap of the iron core of the superconducting magnet. The aluminum billets are rotated by a driving motor. The magnetic flux density was 0.3 T. Fig. 8 shows the electromagnetic torque measurement system for aluminum billets. The electric power meter (ACR220E(L)) is essential for real-time monitoring, which provides the power and current of the AC converter (RNBF-630D/380 and RNBF-200D/380, Shanghai, China) to LabVIEW software.

C. VALIDATION OF NUMERICAL MODEL

The experimental measurement of electromagnetic torque and power were compared with the simulated model shown in Fig. 2. During the experiment, the temperature of the aluminum billet was raised from room temperature (28 °C) to 450 °C, in approximately 12 minutes. The curves of electromagnetic torque and resistive heating power, as a function of rotational speed from 0 rpm to 350 rpm, are shown in Fig. 9. At the stable rotational speed of 350 rpm, when the actual heating process occurs, both the electromagnetic torque and resistive heating power increase with heating time. Note these are not shown in Fig. 9. The simulation data of electromagnetic torque and resistive heating power matches closely with the experimental data. The comparison shows the maximum error of electromagnetic torque is 6% at 240 rpm.

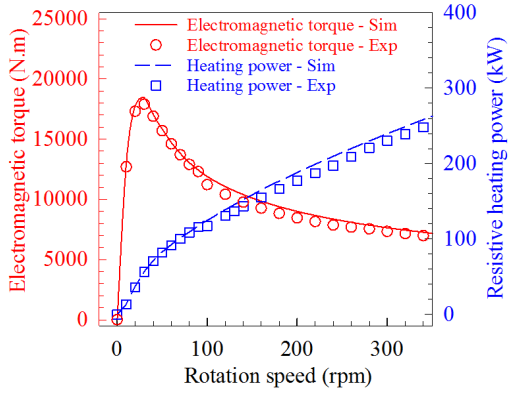

FIGURE 9. Comparison of experimental and simulation results of electromagnetic torque and resistive heating power for the Φ446 mm × 1335 mm aluminum billet in B = 0.3 T.

The experimental and simulation data for the electromagnetic torque are 7,850 N·m and 8,355 N·m at 240 rpm, respectively. For resistive heating power they are 197 kW and 210 kW at 240 rpm, respectively.

IV. ELECTROMAGNETIC TORQUE CHARACTERISTICS

The electromagnetic torque characteristic is significant for considering the driving system solution of the superconducting DC induction heater. In this section, we explore five key relative parameters with the electromagnetic torque. To compare the peak electromagnetic torque T_{peak} and stable torque T_{stable}, the ratio of peak to stable torque, at a high rotation speed, is used to represent the peak torque effect of billet.

A. BILLET DIAMETER

We analyzed the electromagnetic torque of aluminum billets with diameters up to 640 mm. The transverse magnetic field was 0.5 T, and all billets were of length 1500 mm. We calculated the dependence of electromagnetic torque on the rotational speed, and obtained the peak and stable (at 500 rpm) electromagnetic torque. The peak electromagnetic torques of Φ150 mm, Φ300 mm, and Φ640 mm billets were 4,845 N·m, 18,581 N·m, and 85,465 N·m, respectively, as shown in Fig. 10(a). The electromagnetic torque of the Φ40 mm aluminum billet increases with rotational speed up to ∼3000 rpm, and has no peak electromagnetic torque phenomenon. The resistive heating power of all aluminum billets increase with increasing rotational speed, as shown in Fig. 10(b). The slopes of the power curves for Φ150 mm, Φ300 mm, Φ640 mm are greater than 1, due to the rapid increase of torque. Note that the slope value of the heating power curve for the Φ40 mm billet is less than 1.

Fig. 11 shows how the peak and stable (at 500 rpm) electromagnetic torques vary with billet diameter. The peak electromagnetic torque increases with increasing billet diameter. Therefore, peak torque is much more of an issue for aluminum billets with larger diameters. The stable torque curve is approximately linear, with a slope of ∼51, as shown in Fig. 11(a). Whereas the peak electromagnetic torque curve

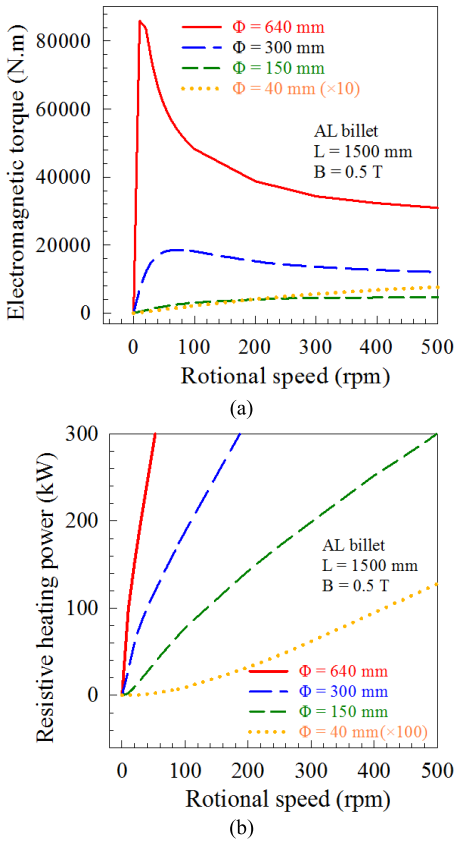

FIGURE 10. (a) Electromagnetic torque and (b) resistive heating power for aluminum billets with different diameters; with length 1500 mm in B = 0.5 T.

is nonlinear. As shown in Fig. 11(b), the corresponding rotation speed of peak electromagnetic torque *npeak* decreases nonlinearly, from 3000 rpm to 10 rpm. For diameters less than 200 mm, the peak electromagnetic torque effect is not significant. For Φ300 mm billets T_{peak} /T_{stable} is 1.54. This rises to $T_{peak}/T_{stable} = 2.8$ for Φ640 mm billets, which poses a great challenge for the driving system design in superconducting DC induction heaters. This is because the driving system will need to overcome the peak electromagnetic torque at low rotational speeds.

B. BILLET LENGTH

We analyzed the electromagnetic torque of aluminum billets with varying lengths of 0-2000 mm. The electromagnetic torque and power results are shown in Fig. 12. Here the transverse magnetic field was 0.5 T, and all aluminum billets had the same diameter: Φ300 mm. We calculated the dependence of electromagnetic torque on the rotational speed, and obtained the peak and stable (at 500 rpm) electromagnetic torque. The peak electromagnetic torques for lengths 100 mm, 500 mm, 1000 mm, and 1500 mm were 1,292 N·m, 6,460 N·m, 12,920 N·m, and 18,581 N·m, respectively. The resistive heating power values of all aluminum billet lengths increase with increasing rotational speed. Fig. 12(b) shows

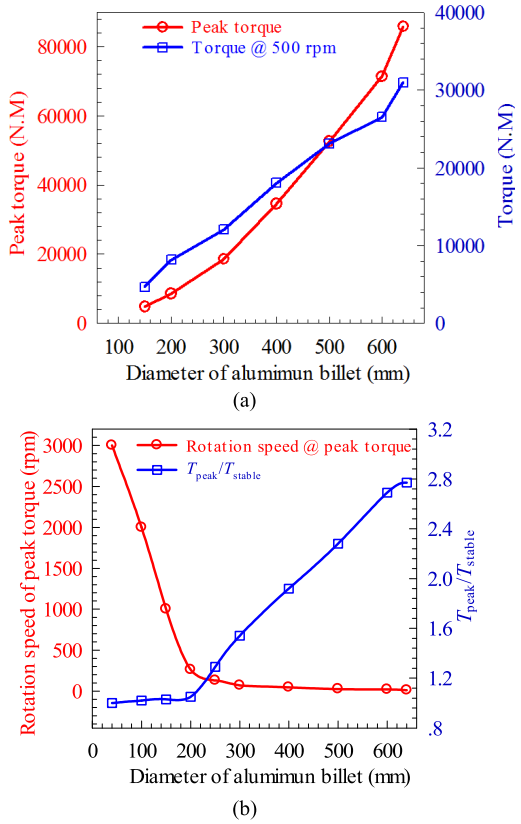

FIGURE 11. Peak and stable (at 500 rpm) electromagnetic torque as a function of aluminum billet diameter, with length 1500 mm and B = 0.5 T. (a) Peak and stable torque curves, and (b) rotational speed of peak electromagnetic torque and the T_{peak}/T_{stable} ratio curves.

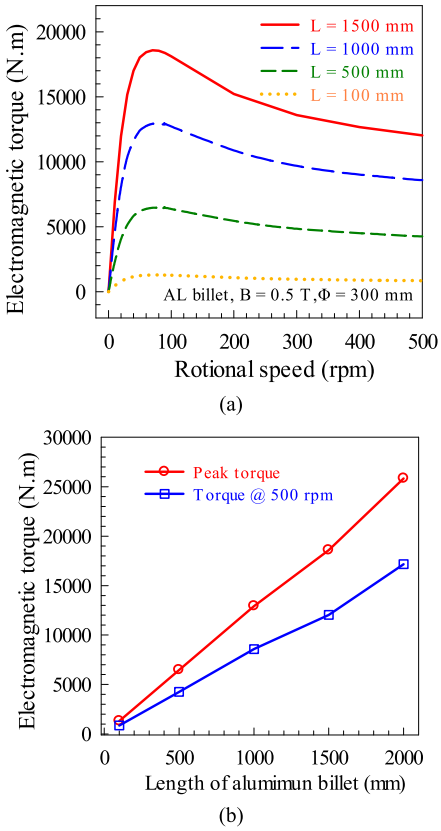

FIGURE 12. Electromagnetic torque for different aluminum billet lengths, with Φ300 mm and B = 0.5 T. (a) Electromagnetic torque curves for different aluminum lengths, and (b) peak and stable electromagnetic torque curves.

peak torque and stable electromagnetic torque variation with different aluminum billet lengths. The peak electromagnetic torque increases linearly with increasing billet diameter. The stable torque curve is also linear. The slope of the peak and stable torque curves are 8.4 and 12.7, respectively. The T_{peak}/T_{stable} ratio for lengths 100 mm, 500 mm, 1000 mm, and 1500 mm are all constant at 1.5.

C. MAGNETIC FLUX DENSITY

We analyzed the electromagnetic torque in a magnetic flux density range of 0-1 T. The electromagnetic torque and power results are shown in Fig. 13. Here, all the aluminum billets have the same diameter and length: Φ640 mm and 1,500 mm, respectively. The peak and stable (at 500 rpm) electromagnetic torque were obtained as a function of magnetic flux density. The peak electromagnetic torques for 0.1 T, 0.3 T, 0.5 T, and 1 T are 3,470 N·m, 18,302 N·m, 50,421 N·m, and 205,286 N·m, respectively, as shown in Fig. 13(a). The resistive heating power curves increase nonlinearly with increasing magnetic flux density, as shown in Fig. 13(b). The 1st order value of the 4th order polynomial fitted to the 1 T power curve is 17, which is much higher than that of the 0.1 T power curve: 0.067.

Fig. 14 shows the peak and stable electromagnetic torque variation with magnetic flux density, over a 0-1 T range. The peak electromagnetic torque rapidly increases nonlinearly with increasing of billet diameter. 2nd order polynomials were fitted to the peak and stable torque curves. The R-squared values of the polynomial fitting were 0.99 for both curves. As shown in Fig. 14(b), the corresponding rotational speed n_{peak} of the peak electromagnetic torque decreases nonlinearly with increasing magnetic flux density, from 0.1 T to 1 T. When the magnetic flux density is 0.1 T and 1 T, the corresponding rotational speeds n_{peak} are 12 rpm and 14 rpm, respectively. The corresponding rotational speed effect is not significant. The T_{peak} /T_{stable} ratio for magnetic flux densities of 0.1 T, 0.5 T, and 1 T, are 9.4, 1.6, and 1.4, as shown in Fig. 11(b). The T_{peak} /T_{stable} ratio decreases with increasing magnetic flux density. This is useful for optimizing the magnetic flux density of the superconducting coil. The analysis result is also useful for the design of driving system in superconducting DC induction heater.

D. BILLET MATERIAL

The effect of different billet materials on the peak electromagnetic torque is explored in this section. Superconducting DC induction heaters are also suitable for various materials,

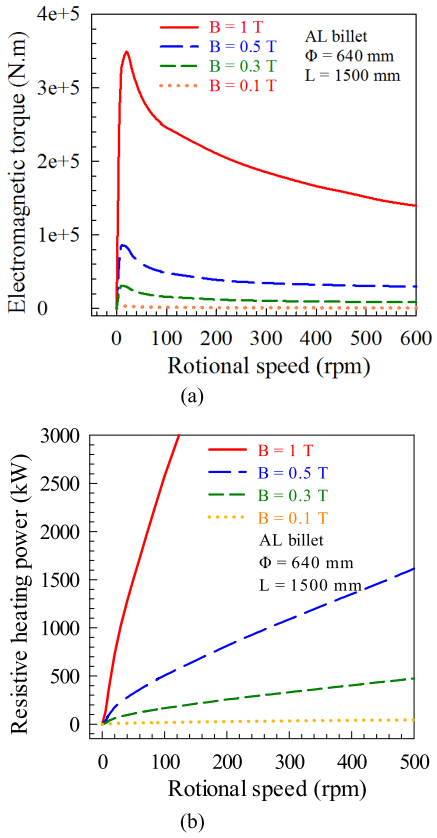

FIGURE 13. Electromagnetic torque and resistive heating power at different magnetic flux densities, using an aluminum billet (Φ446 mm × 1500 mm). (a) Electromagnetic torque curves for different magnetic flux densities: B = 0.1 T, 0.3 T, 0.5 T, and 1 T. (b) Resistive heating power curves.

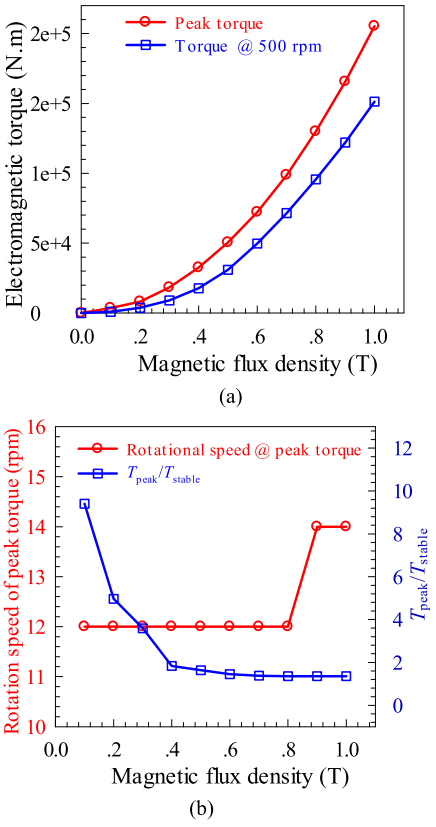

FIGURE 14. Peak and stable electromagnetic torque for different aluminum magnetic flux densities, using an aluminum billet (Φ446 mm × 1500 mm)and B = 0.5 T. (a) Peak and stable torque curves. (b) Rotational speed of peak electromagnetic torque and T_{peak} / T_{stable} ratio curves.

such as copper, titanium alloy, stainless steel, etc. Copper and titanium alloy (Ti-6Al-2Sn-4Zr-2Mo) billets were analyzed and compared. Fig. 15 shows the electrical conductivity of aluminum, copper and titanium alloy. The electrical conductivity of aluminum, copper, and titanium alloy at 293 K are 3.72 × 10^7 S/m, 3.87 × 10^7 S/m, and 5.9 × 10^6 S/m, respectively. Here, all billets were the same size (Φ640 mm × 1500 mm), measured with B = 0.5 T. The peak electromagnetic torque of aluminum and copper are 85,465 N·m and 84,570 N·m, respectively, as shown in Fig. 16(a). The corresponding rotational speed n_{peak} at the peak electromagnetic torque are 10 rpm and 8 rpm, respectively. The electromagnetic torque of the titanium alloy billet increases with the rotational speed up to 500 rpm, showing no peak electromagnetic torque phenomenon.

E. ELECTRICAL CONDUCTIVITY

In this section, the effect of electrical conductivity, on the peak electromagnetic torque, was studied. and other material parameters are same with the aluminum. The electromagnetic torque and power results are shown in Fig. 17. Here, the transverse magnetic field was 0.5 T, and all billets had the same size: Φ640 mm × 1500 mm. The peak electromagnetic

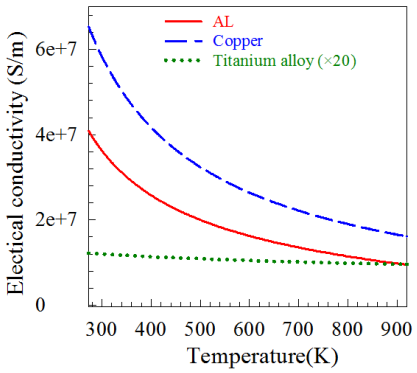

FIGURE 15. Temperature dependence of electrical conductivity curves of aluminum, copper and titanium alloy from the FEM simulation.

torques for 1 × 10^7 S/m and 1 × 10^8 S/m are 88,237 N·m at 50 rpm, and 87,573 N·m at 5 rpm, respectively, as shown in Fig. 17(a). The electromagnetic torque for 1 × 10^5 S/m increases with rotational speed up to 500 rpm. There is no peak electromagnetic torque phenomenon, which is similar to titanium alloy. The resistive heating power for all electrical conductivities increase with increasing rotational speed, as shown in Fig. 17(b). In the low rotational speed range, below 100 rpm, the slope value of resistive heating power for

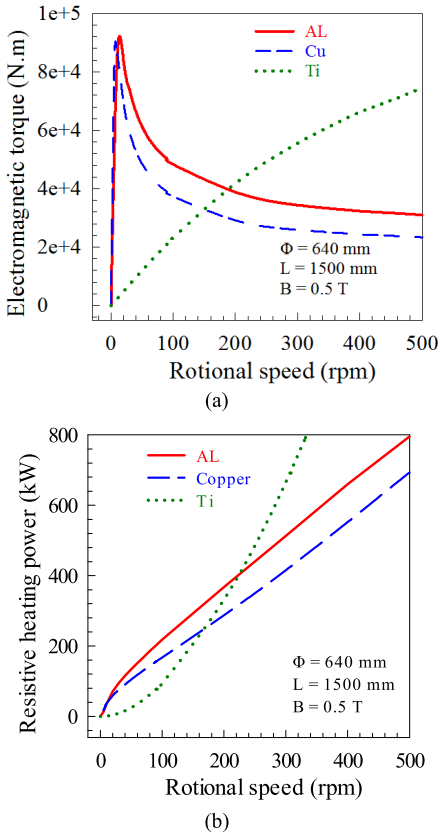

FIGURE 16. Electromagnetic torque and resistive heating power for different materials, with Φ640 mm × 1500 mm billets and B = 0.5 T., (a) Electromagnetic torque curves and (b) resistive heating power curves.

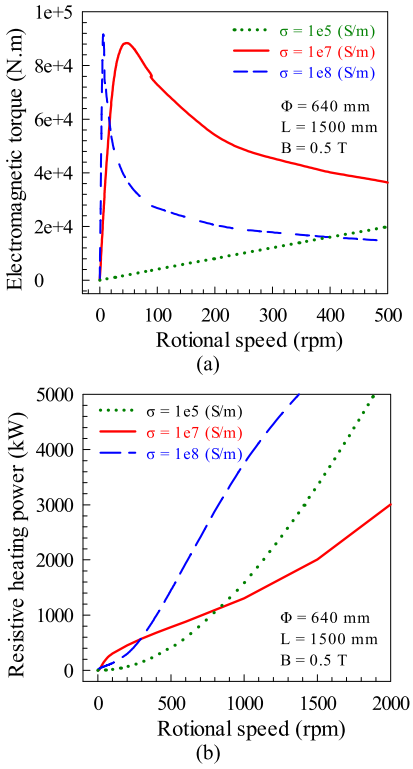

FIGURE 17. (a) Electromagnetic torque curves and (b) resistive heating power curves, for different electrical conductivities, for Φ640 mm × 1500 mm billets and B = 0.5 T.

$\sigma = 1 \times 10^7$ S/m is higher than that of $\sigma = 1 \times 10^5$ S/m and $\sigma = 1 \times 10^8$ S/m. The resistive heating power for 1×10^5 S/m, 1×10^7 S/m, and 1×10^8 S/m at 100 rpm, are 17 kW, 302 kW, and 129 kW, respectively. In the high rotational speed range, above 100 rpm, the slope values for $\sigma = 1 \times 10^5$ S/m and $\sigma = 1 \times 10^8$ S/m are higher than that of $\sigma = 1 \times 10^7$ S/m. The resistive heating power for 1×10^5 S/m, 1×10^7 S/m, and 1×10^8 S/m at 500 rpm, are 412 kW, 781 kW, and 1454 kW, respectively.

Fig. 18 shows the variation in the peak and stable torques at 500 rpm, for different electrical conductivities $\sim 10^4 - 10^{10}$S/m. The peak electromagnetic torque remains almost same at 87,573-88,430 N·m over the range of $10^5 - 10^8$S/m. The peak electromagnetic torque decreases nonlinearly with increasing electrical conductivity above 10^8S/m. The minimum peak electromagnetic torque is 9,278 N·m at 1×10^{10}S/m. As electrical conductivity increases, the stable torque increases before beginning to decrease after reaching a maximum point, 51,884 N·m at 1×10^6S/m, as shown in Fig. 18(a). As shown in Fig. 18(b), the corresponding rotational speed n_{peak} of the peak electromagnetic torque decreases nonlinearly, from 5000 rpm to 5 rpm, with increasing electrical conductivity. When the electrical conductivity is less than 1×10^7S/m, the effect on the corresponding rotation speed is significant. Whereas when the electrical conductivity is more than 1×10^7S/m, the corresponding rotation speed remains almost the same at 5-10 rpm. The $T_{\text{peak}}/T_{\text{stable}}$ ratio increases nonlinearly over the range of $10^6 - 10^{10}$S/m.

V. AUXILIARY MOTOR SOLUTION OF A DRIVING SYSTEM FOR THE PEAK ELECTROMAGNETIC TORQUE

A driving system, consisting of a main motor and an auxiliary motor, was developed to rotate aluminum billets in a 1 MW superconducting DC induction heater, as shown in Fig. 19. The key idea of this driving system is to use an auxiliary motor to provide extra torque for the billet during low rotational speed. This ensures that the main motor can start-up successfully. The range of billets used for the 1 MW superconducting DC induction heater have diameters of 200-446 mm and lengths of 800-1500 mm. This design solution has advantages in both reliability and reduced cost, compared to a high-power capability motor solution. The details of the motors and gearboxes are shown in Table 1. The main motor was selected according to the power and torque of the billet at the top-rated rotation speed. A gearbox, with ratio 3.15:1, is engaged with the main motor to increase the output torque, as well as decrease the output rotation speed. The auxiliary motor provides extra torque at low rotation speed, using an auxiliary gearbox with a high ratio (10:1), whose connection with the billets is controlled by a clutch.

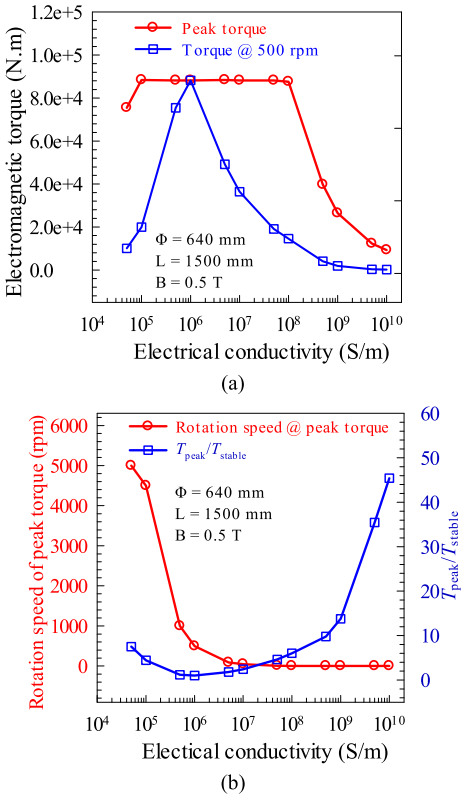

FIGURE 18. (a) Peak and stable electromagnetic torque curves. (b) Rotational speed of peak electromagnetic torque and T_{peak}/T_{stable} ratio curves, with different electrical conductivities for Φ640 mm × 1500 mm billets and B = 0.5 T.

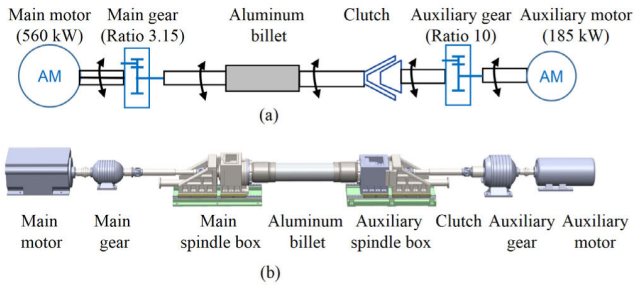

FIGURE 19. Schematic of the driving system based on a main and auxiliary motor for a 1 MW HTS DC induction heater.

Fig. 20 shows the control flowchart of an independent heating period. First, the main and auxiliary motors start synchronously. The auxiliary motor is engaged to the aluminum billets through the clutch, until the main motor is capable of driving the aluminum billet independently. After the aluminum billet reaches 130 rpm, the clutch is disengaged and the auxiliary motor is stopped. The main motor rotates the aluminum billets independently, to the top-rated rotation speed. The aluminum billet temperature increases to the target temperature of 450 °C during the heating period at the top speed, which is approximately 12 minutes.

Fig. 21 shows measurements of the electromagnetic torque and power of the main and auxiliary motors during a heating

TABLE 1. Specification of driving system for the 1MW superconducting DC induction heater.

Parameter	Main motor	Auxiliary motor
Rated power	560 kW	185 kW
Rated speed	1485 rpm	990 rpm
Rated frequency	50 Hz	50 Hz
Rated voltage	380 V	380 V
Rated current	991 A	347 A
Constant torque range	3565 N·m	1776 N·m
Maximum/rated torque	1.8	2.8
Power factor cosΦ	0.91	0.86
Gear ratio	3.15	10

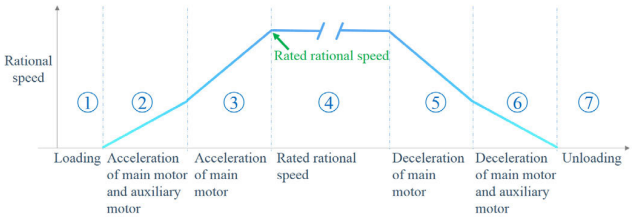

FIGURE 20. Control flowchart of the main and auxiliary motors solution to achieve peak electromagnetic torque.

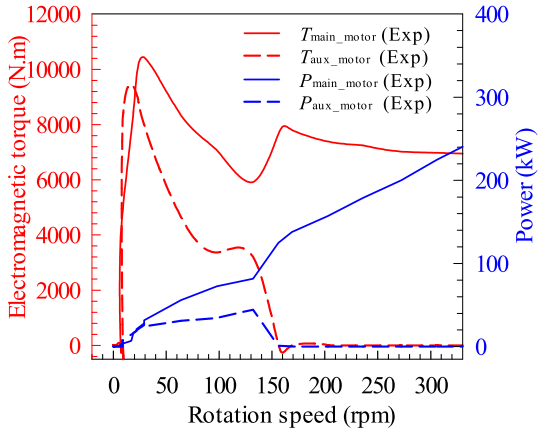

FIGURE 21. Output torque and power of the main and auxiliary motors during a heating cycle for a Φ446 mm ×1335 mm aluminum billet, with B = 0.3 T. Here, T_{main_motor} and P_{main_motor} are the output torque and power of the main motor, respectively. T_{aux_motor} and P_{aux_motor} are the output torque and power of the auxiliary motor, respectively.

cycle. At the peak load torque point (29 rpm), the main motor contributes a torque of 10,457 N·m, while the auxiliary motor contributes 9092 N·m. Thus, the total output torque from this driving system is 19,549 N·m, which meets the load torque requirement of 18,841 N·m. Therefore, the practicability of this driving system, developed for this 1 MW DC induction heater, has been validated experimentally.

VI. CONCLUSION

This paper presents the peak electromagnetic torque characteristics that occur at low rotation speeds. Five relative param-

eters were analyzed. A numerical FEM model was compared with experimental measurements using a superconducting DC induction heater. The conclusions are as follows:

1) The peak electromagnetic torque increases nonlinearly with increasing billet diameter. Although, for diameters smaller than 200 mm, the peak electromagnetic torque effect is not significant. The T_{peak}/T_{stable} ratio is 2.8 for Φ640 mm aluminum billets in B = 0.5 T.

2) The peak electromagnetic torque increases linearly with increasing billet length. The stable (at 500 rpm) torque curve is also linear. The slope values of the peak and stable torque curves are constant, at 8.4 and 12.7, respectively, as a function of billet length, with Φ300 mm and B = 0.5 T.

3) The T_{peak}/T_{stable} ratio decreases nonlinearly with increasing magnetic flux density.

4) The peak electromagnetic torque of aluminum and copper are 85,465 N·m at 10 rpm, and 84,570 N·m at 8 rpm, respectively. The electromagnetic torque of the titanium alloy billet increases with rotational speed, up to 500 rpm, such that there is no peak electromagnetic torque phenomenon.

5) When the electrical conductivity is above 1×10^7S/m, the corresponding rotation speed remains almost constant at 5-10 rpm. The T_{peak}/T_{stable} ratio increases nonlinearly over the range $10^6 - 10^{10}$S/m.

The feasibility of an auxiliary motor driving system, developed for a 1 MW superconducting DC induction heater, was validated. These results are useful for guiding the driving system design of superconducting DC induction heaters.

REFERENCES

[1] S. Hahn, K. Kim, K. Kim, X. Hu, T. Painter, I. Dixon, S. Kim, K. R. Bhattarai, S. Noguchi, J. Jaroszynski, and D. C. Larbalestier, "45.5-tesla direct-current magnetic field generated with a high-temperature superconducting magnet," *Nature*, vol. 570, no. 7762, pp. 496–499, Jun. 2019.

[2] M. Runde, N. Magnusson, C. Fulbier, and C. Buhrer, "Commercial induction heaters with high–temperature superconductor coils," *IEEE Trans. Appl. Supercond.*, vol. 21, no. 3, pp. 1379–1383, Jun. 2011.

[3] A. Stenvall, N. Magnusson, Z. Jelinek, G. Grasso, I. Hiltunen, A. Korpela, J. Lehtonen, R. Mikkonen, and M. Runde, "Electromagnetic viewpoints on a 200kW MgB_2 induction heater," *Phys. C, Supercond.*, vol. 468, no. 6, pp. 487–491, Mar. 2008.

[4] J. Li, R. Xiong, Q. Yang, F. Liang, M. Zhang, and W. Yuan, "Design/test of a hybrid energy storage system for primary frequency control using a dynamic droop method in an isolated microgrid power system," *Appl. Energy*, vol. 201, pp. 257–269, Sep. 2017.

[5] J. Li, X. Wang, Z. Zhang, S. Le Blond, Q. Yang, M. Zhang, and W. Yuan, "Analysis of a new design of the hybrid energy storage system used in the residential m-CHP systems," *Appl. Energy*, vol. 187, pp. 169–179, Feb. 2017.

[6] D. C. Van Der Laan, J. D. Weiss, C. H. Kim, L. Graber, and S. Pamidi, "Development of CORC cables for helium gas cooled power transmission and fault current limiting applications," *Supercond. Sci. Technol.*, vol. 31, no. 8, Aug. 2018, Art. no. 085011.

[7] Y. Wang, J. Zheng, Z. Zhu, M. Zhang, and W. Yuan, "Quench behavior of high-temperature superconductor (RE)$Ba_2Cu_3O_x$ CORC cable," *J. Phys. D, Appl. Phys.*, vol. 52, no. 34, Aug. 2019, Art. no. 345303.

[8] J. Ma, J. Sheng, Z. H. Yao, H. Y. Gan, H. J. Li, X. Z. Ai, Z. Y. Li, Z. Jin, and Z. Hong, "Experimental and numerical study of a DC induction heater prototype with an adjustable air gap structure," *IEEE Trans. Appl. Supercond.*, vol. 26, no. 4, pp. 1–5, Jun. 2016.

[9] H. Gao, Y. Wang, D. Q. Xu, Y. Shi, Z. Y. Li, Z. Jin, and Z. Hong, "Heating characteristics of a HTS DC induction heater for aluminum billets," *IEEE Trans. Appl. Supercond.*, vol. 25, no. 3, Jun. 2015, Art. no. 4600904.

[10] J. Yang, H. Gao, Y. W. Wang, D. Q. Xu, Z. Hong, Z. Jin, and Z. Y. Li, "Design and experimental results of a DC induction heater prototype for aluminum billets," *IEEE Trans. Appl. Supercond.*, vol. 24, no. 3, Jun. 2014, Art. no. 0500704.

[11] J. Ma, J. Geng, and T. A. Coombs, "Flux pumping for non-insulated and metal-insulated HTS coils," *Supercond. Sci. Technol.*, vol. 31, no. 1, Jan. 2018, Art. no. 015018.

[12] J. Ma, J. Geng, J. Gawith, H. Zhang, C. Li, B. Shen, Q. Dong, J. Yang, J. Chen, Z. Li, and T. A. Coombs, "Rotating permanent magnets based flux pump for HTS no–insulation coil," *IEEE Trans. Appl. Supercond.*, vol. 29, no. 5, pp. 1–6, Aug. 2019.

[13] H. Song and Y. Wang, "Simulations of non-uniform behaviors of multiple no–insulation (RE)$Ba_2Cu_3O_{7-x}$ HTS pancake coils during charging and discharging," *IEEE Trans. Appl. Supercond.*, vol. 26, no. 4, Jun. 2016, Art. no. 4700105.

[14] H. Song, D. Hazelton, D. Fukushima, and P. Brownsey, "Engineering design and novel winding approaches in developing high quality HTS REBCO coils," *IEEE Trans. Appl. Supercond.*, vol. 27, no. 4, Jun. 2017, Art. no. 4601305.

[15] H. Song, E. E. Burkhardt, T. Borden, S. Chouhan, D. Cole, D. Georgobiani, M. Hausmann, M. Patil, M. Portillo, R. Ronningen, R. Swanson, Y. Xu, and A. Zeller, "Design and engineering of an HTS dipole in the FRIB fragment separator," *IEEE Trans. Appl. Supercond.*, vol. 25, no. 3, pp. 1–6, Jun. 2015.

[16] Y. Wang, H. Song, D. Xu, Z. Y. Li, Z. Jin, and Z. Hong, "An equivalent circuit grid model for no-insulation HTS pancake coils," *Supercond. Sci. Technol.*, vol. 28, no. 4, Apr. 2015, Art. no. 045017.

[17] Y. Wang, W. K. Chan, and J. Schwartz, "Self-protection mechanisms in no-insulation (RE)$Ba_2Cu_3O_x$ high temperature superconductor pancake coils," *Supercond. Sci. Technol.*, vol. 29, no. 4, Apr. 2016, Art. no. 045007.

[18] Y. Wang, M. Zhang, F. Grilli, Z. Zhu, and W. Yuan, "Study of the magnetization loss of CORC cables using a 3D T—A formulation," *Supercond. Sci. Technol.*, vol. 32, no. 2, Feb. 2019, Art. no. 025003.

[19] Y. Wang, Y. Ping, K. Li, H. Song, J. Yang, C. Ma, Z. Jin, and Z. Hong, "Analysis and comparison between no-insulation and metallic insulation REBCO magnet for the engineering design of a 1-MW DC induction heater," *IEEE Trans. Appl. Supercond.*, vol. 27, no. 4, Jun. 2017, Art. no. 3700105.

[20] P. Yang, K. Li, Y. Wang, L. Wang, Q. Wu, A. Huang, Z. Hong, G. Jiang, and Z. Jin, "Quench protection system of a 1 MW high temperature superconductor DC induction heater," *IEEE Trans. Appl. Supercond.*, vol. 29, no. 5, pp. 1–6, Aug. 2019.

[21] P. Yang, Y. Wang, D. Qiu, T. Chang, H. Ma, J. Zhu, Z. Jin, and Z. Hong, "Design and fabrication of a 1-MW high–temperature superconductor DC induction heater," *IEEE Trans. Appl. Supercond.*, vol. 28, no. 4, Jun. 2018, Art. no. 3700305.

[22] T. Lubin and A. Rezzoug, "Improved 3-D analytical model for axial–flux eddy–current couplings with curvature effects," *IEEE Trans. Magn.*, vol. 53, no. 9, pp. 1–9, Sep. 2017.

[23] T. Lubin, S. Mezani, and A. Rezzoug, "Simple analytical expressions for the force and torque of axial magnetic couplings," *IEEE Trans. Energy Convers.*, vol. 27, no. 2, pp. 536–546, Jun. 2012.

[24] Y. Ping, W. Yawei, T. Chang, H. Ma, L. Zhuyong, J. Zhijian, and H. Zhiyong, "Start-up strategy using flywheel energy storage for superconducting DC induction heater," *Compel*, vol. 36, no. 4, pp. 1298–1309, 2017.

[25] J. Choi, T. Kim, C.-K. Lee, D.-S. Jeon, G.-W. Park, S. Cho, M. Park, I.-K. Yu, and M. Iwakuma, "Commercial design and operating characteristics of a 300 kW superconducting induction heater (SIH) based on HTS magnets," *IEEE Trans. Appl. Supercond.*, vol. 29, no. 5, pp. 1–5, Aug. 2019.

[26] J. Choi, S.-K. Kim, K. Kim, M. Park, I.-K. Yu, S. Kim, and K. Sim, "Design and performance evaluation of a multi–purpose HTS DC induction heating machine for industrial applications," *IEEE Trans. Appl. Supercond.*, vol. 25, no. 3, Jun. 2015, Art. no. 3700105.

[27] J. Choi, C. S. Hwang, C. K. Lee, S. K. Kim, M. Park, and I. K. Yu, "Performance test of a metal insulated HTS magnet with conduction cooling," *J. Phys., Conf. Ser.*, vol. 871, Jul. 2017, Art. no. 012086.

[28] J. Choi, B. S. Go, S. K. Kim, S. H. Cho, H. J. Park, H. J. Moon, K. Sim, M. Park, and I. K. Yu, "Economic feasibility study of an HTS DC induction furnace," *IEEE Trans. Appl. Supercond.*, vol. 26, no. 4, Jun. 2016, Art. no. 3700804.

[29] J. Choi, C.-K. Lee, S. Cho, M. Park, I.-K. Yu, and M. Iwakuma, "Recent development and research activities of induction heater with high-T_C superconducting magnets for commercialization," *SN Appl. Sci.*, vol. 1, no. 1, p. 59, 2018.
[30] J. Choi, S. K. Kim, S. Kim, K. Sim, M. Park, and I. K. Yu, "Characteristic analysis of a sample HTS magnet for design of a 300 kW HTS DC induction furnace," *IEEE Trans. Appl. Supercond.*, vol. 26, no. 3, Apr. 2016, Art. no. 3700405.
[31] J. Choi, K. Kim, M. Park, I.-K. Yu, S. Kim, and K. Sim, "Fabrication and testing of a prototype 10-kW class HTS DC induction heating machine," *J. Supercond. Novel Magn.*, vol. 28, no. 2, pp. 657–661, Feb. 2015.
[32] J. Choi, K. Kim, M. Park, I.-K. Yu, S. Kim, K. Sim, and H.-J. Kim, "Practical design and operating characteristic analysis of a 10 kW HTS DC induction heating machine," *Phys. C, Supercond. Appl.*, vol. 504, pp. 120–126, Sep. 2014.
[33] S. Choi, H. C. Jo, Y. J. Hwang, S. Hahn, and T. K. Ko, "A study on the no insulation winding method of the HTS coil," *IEEE Trans. Appl. Supercond.*, vol. 22, no. 3, Jun. 2012, Art. no. 4904004.
[34] Y. Hyuck Choi, O. Jun Kwon, Y.-G. Kim, J.-B. Song, J. H. Kim, H.-M. Kim, and H. Lee, "Thermal quench behaviors of no–insulation coils wound using GdBCO coated conductor tapes with various lamination materials," *IEEE Trans. Appl. Supercond.*, vol. 24, no. 3, pp. 1–5, Jun. 2014.
[35] J. H. Choi, Y. H. Choi, D.-H. Kang, Y. Park, J.-B. Song, S.-K. Ha, M. Park, and H. Lee, "Investigation of the key factors affecting the permanent damage of the REBCO coated conductor in overcurrent condition," *IEEE Trans. Appl. Supercond.*, vol. 25, no. 3, pp. 1–5, Jun. 2015.
[36] Y. Wang, J. Wen, Z. Y. Li, Z. Jin, and Z. Hong, "Design of a HTS magnet with iron core for DC induction heater," *IEEE Trans. Appl. Supercond.*, vol. 24, no. 3, Jun. 2014, Art. no. 4602005.
[37] Y. Wang, J. Yang, Z. Y. Li, Z. Jin, and Z. Hong, "Study on a numerical method for calculating the heating process of HTS DC induction heater," *IEEE Trans. Appl. Supercond.*, vol. 24, no. 3, Jun. 2014, Art. no. 0501105.
[38] Y. Wang, H. Gao, Z. Li, Y. Ping, Z. Jin, and Z. Hong, "Study of the temperature uniformity of aluminium billets heated by superconducting DC induction heaters," *Compel*, vol. 34, no. 1, pp. 357–370, Jan. 2015.
[39] Y. Wang, D. Xu, H. Sun, X. Liu, J. Sheng, K. Li, Z. Hong, Z. Jin, and Z. Li, "Study on no–insulation HTS pancake coils with iron core for superconducting DC induction heaters," *IEEE Trans. Appl. Supercond.*, vol. 25, no. 3, Jun. 2015, Art. no. 4600305.
[40] Y. Wang and H. Song, "Influence of turn-to-turn resistivity and coil geometrical size on charging characteristics of no-electrical-insulation REBCO pancake coils," *Supercond. Sci. Technol.*, vol. 29, no. 7, Jul. 2016, Art. no. 075006.
[41] K. Li, Y. Wang, P. Yang, C. Ma, D. Qiu, Y. Pan, Z. Li, Z. Jin, and Z. Hong, "Coil voltage pulse at the beginning of the fast discharge operation of no–insulation REBCO coils," *IEEE Trans. Appl. Supercond.*, vol. 27, no. 4, pp. 1–5, Jun. 2017.
[42] Y. Wang, H. Song, W. Yuan, Z. Jin, and Z. Hong, "Ramping turn-to-turn loss and magnetization loss of a No–Insulation (RE)$Ba_2Cu_3O_x$ high temperature superconductor pancake coil," *J. Appl. Phys.*, vol. 121, no. 11, Mar. 2017, Art. no. 113903.
[43] Y. Wang, M. Zhang, W. Yuan, Z. Hong, Z. Jin, and H. Song, "Non-uniform ramping losses and thermal optimization with turn-to-turn resistivity grading in a (RE)$Ba_2Cu_3O_x$ magnet consisting of multiple no-insulation pancake coils," *J. Appl. Phys.*, vol. 122, no. 5, Aug. 2017, Art. no. 053902.
[44] P. Yang, Y. Wang, J. Sheng, F. Wang, D. Qiu, L. B. Wang, Z. Jin, and Z. Hong, "Experimental and numerical study of quench characteristics of nonuniform REBCO–coated conductors," *IEEE Trans. Appl. Supercond.*, vol. 27, no. 4, Jun. 2017, Art. no. 6602406.
[45] F. Berg, J. Palmer, P. Miller, and G. Dodds, "HTS system and component targets for a distributed aircraft propulsion system," *IEEE Trans. Appl. Supercond.*, vol. 27, no. 4, pp. 1–7, Jun. 2017.
[46] D. Zhang, G. Zhang, L. Lin, L. Xiao, N. Song, L. Jing, X. Wang, S. Liang, Q. Li, Y. Teng, and J. Zhang, "Research on the conduction–cooled YBCO magnet for an MW class induction heating system," *IEEE Trans. Appl. Supercond.*, vol. 28, no. 3, pp. 1–5, Apr. 2018.
[47] A. Morandi, M. Fabbri, and P. Ribani, "Design of a superconducting saddle magnet for DC induction heating of aluminum billets," *IEEE Trans. Appl. Supercond.*, vol. 18, no. 2, pp. 816–819, Jun. 2008.
[48] R. Araneo, F. Dughiero, M. Fabbri, M. Forzan, A. Geri, A. Morandi, S. Lupi, P. Ribani, and G. Veca, "Electromagnetic and thermal analysis of the induction heating of aluminum billets rotating in DC magnetic field," *Compel*, vol. 27, no. 2, pp. 467–479, Mar. 2008.
[49] M. Fabbri, A. Morandi, and P. Luigi Ribani, "DC induction heating of aluminum billets using superconducting magnets," *Compel*, vol. 27, no. 2, pp. 480–490, Mar. 2008.
[50] M. Fabbri, M. Forzan, S. Lupi, A. Morandi, and P. L. Ribani, "Experimental and numerical analysis of DC induction heating of aluminum billets," *IEEE Trans. Magn.*, vol. 45, no. 1, pp. 192–200, Jan. 2009.

PING YANG was born in Jiangxi, China, in 1980. He received the B.S. degree in materials science and engineering from Northwestern Polytechnical University, Xi'an, China, in 2002, and the Ph.D. degree in electrical engineering from Shanghai Jiao Tong University, Shanghai, China, in 2017. His research focuses on superconducting dc induction heater.

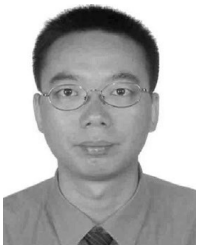

SHAOTAO DAI was born in Jiangxi, China, in 1972. He received the B.S. and M.E. degrees from Central South University, Changsha, China, in 1994 and 1997, respectively, and the Ph.D. degree from the Graduate School of Chinese Academy of Sciences, in 2010. He was a Professor with Beijing Jiaotong University, Beijing, China. He was a member of Superconducting Applied Technology Professional Committee of China Electrotechnical Society. He is leading the research team in the area applied the application of HTS, including cables, fault current limiters, energy storage, machines, transformer, and power transmission lines.

TAO MA was born in Hubei, China, in 1984. He received the B.S. degree in automation specialty and the Ph.D. degree in control science and engineering from the Beijing Institute of Technology University, Beijing, China, in 2006 and 2011, respectively. He has been an Associate Professor with Beijing Jiaotong University, Beijing, since 2016.

JIANMIN HUANG received the B.S. degree from Nanchang University, Nanchang, China. He was a Senior Engineer in the application of LED technology, China. He was an Administrator with Postdoctoral Office, Jiangxi Lianchuang Opto-Electronic Science and Technology Company, Ltd., China.

GUOZHONG JIANG was born in Jiangxi, China, in 1961. He received the B.S. degree in solid state physics and the master's degree from Nanjing University, Nanjing, China, in 1982 and 1990, respectively. He was an academic and technical leaders of major disciplines in enjoy special government allowances of Jiangxi province, China. He was a Chief Engineer with Jiangxi Lianchuang Opto-Electronic Science and Technology Company, Ltd., China.

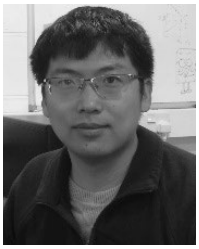

YAWEI WANG was born in Henan, China, in 1987. He received the B.S. degree in electrical engineering from Chongqing University, Chongqing, China, in 2011, and the Ph.D. degree in electrical engineering from Shanghai Jiao Tong University, Shanghai, China, in 2016. His research interests include high temperature superconductor (HTS) cables, HTS machines of electrical aircraft, and high field magnets.

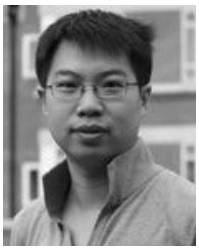

ZHIYONG HONG was born in China, in 1981. He received the B.S. degree in electrical engineering from Shanghai Jiao Tong University, Shanghai, China, in 2003, and the master's and Ph.D. degrees from Cambridge University, in 2007. He was a Professor with Shanghai Jiao Tong University. His research focuses on HTS current limiters, HTS motors, superconducting dc induction heater, machines, transformer, and power transmission lines.

ZHIJIAN JIN was born in China, in 1965. He received the B.S. degree in high voltage engineering from Shanghai Jiao Tong University, Shanghai, China, in 1987, and the master's and Ph.D. degrees from Cambridge University, in 1990 and 1999, respectively. He was a Professor with Shanghai Jiao Tong University. He successively served as the Director of the High Voltage Engineering Research School, the Vice Director of the Electrical Engineering Department, Shanghai Jiao Tong University, and the Deputy Director of the State Energy Smart Grid Research and Development Center.